ACS APPLIED BIO MATERIALS

www.acsabm.org Article

Acoustofection: High-Frequency Vibrational Membrane Permeabilization for Intracellular siRNA Delivery into Nonadherent Cells

Shwathy Ramesan, Amgad R. Rezk, Paula M. Cevaal, Christina Cortez-Jugo, Jori Symons, and Leslie Y. Yeo*

Cite This: *ACS Appl. Bio Mater.* 2021, 4, 2781−2789 Read Online

ACCESS | Metrics & More | Article Recommendations | Supporting Information

ABSTRACT: The internalization of therapeutic molecules into cells—a critical step in enabling a suite of autologous ex vivo gene and cell therapies—is highly regulated by the lipid barrier imposed by the cell membrane. Strategies to increase the efficiency of delivering these exogenous payloads into the cell, while maintaining the integrity of both the therapeutic molecules to be delivered as well as the host cells they are delivered to, are therefore required. This is especially the case for suspension cells that are particularly difficult to transfect. In this work, we show that it is possible to enhance the uptake of short interfering RNA (siRNA) into nonadherent Jurkat and HuT 78 cells with a rapid poration-free method involving high-frequency (MHz order) acoustic excitation. The 2-fold enhancement in gene knockdown is almost comparable with that obtained with conventional nucleofection, which is among the most widely used intracellular delivery methods, but with considerably higher cell viabilities (>91% compared to approximately 76%) owing to the absence of pore formation. The rapid and effective delivery afforded by the platform, together with its low cost and scalability, therefore renders it a potent tool in the cell engineering pipeline.

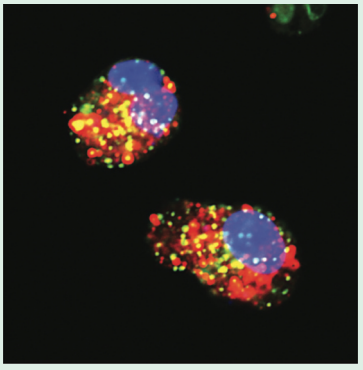

KEYWORDS: *acoustics, nucleic acid, suspension cells, transfection, gene delivery, cell engineering*

1. INTRODUCTION

Advances in gene therapy and editing, cell immunotherapy, and stem cell reprogramming to date have heralded the exciting possibility of ex vivo autologous therapeutics in which a patient's target cells are isolated from their blood or tissue, reengineered in the laboratory, and reinfused to the same patient.[1,2] There is therefore huge anticipation that these breakthroughs will not just revolutionize the treatment of infectious diseases, cancer, and other conditions arising due to genetic mutation but also potentially allow a means for the eradication of infectious transmission by altering the reproductive or characteristic genes within a host.[3] An indispensable step in these techniques is the delivery of molecules such as nucleic acids, proteins, or other therapeutic agents into the cells.

The hydrophobic and apolar nature of the lipid bilayer constituting the cell membrane, in addition to its dynamic structure and selective permeability, nevertheless, poses a formidable barrier that severely restricts such internalization.[2] There has therefore been considerable effort to date in the development of various techniques for facilitating transport through the cell lipid bilayer to deliver a wide range of therapeutic molecules of varying size, surface charge (ζ-potential), and material properties (e.g., hydrophilicity/hydrophobicity)[4,5] into cells. These methods predominantly comprise either biochemical carriers (e.g., viruses, nanoparticles, polymers, etc.) as vehicles to transport their cargo through the cell membrane predominantly through endocytic pathways[6−8] or physical membrane disruption methods that employ the use of external forces to primarily porate the membrane to allow molecular uptake.[1,9]

Biochemical methods often involve extensive preparatory steps and require endosomal escape strategies to avoid accumulation and hence eventual degradation of the therapeutic cargo in the highly acidic and enzyme-rich lysosome environment within the cell.[10] Furthermore, the biochemical carriers that have been found to be the most efficient for transfection are often associated with detrimental effects. Viral vectors, for example, have long been known to trigger immunogenic and carcinogenic responses,[11] whereas polycation carriers such as poly(ethyleneimine) have been found to be cytotoxic to varying degrees.[12] Physical pore forming methods such as electroporation (also known as

Received: January 4, 2021
Accepted: February 19, 2021
Published: March 3, 2021

https://dx.doi.org/10.1021/acsabm.1c00003
ACS Appl. Bio Mater. 2021, 4, 2781−2789

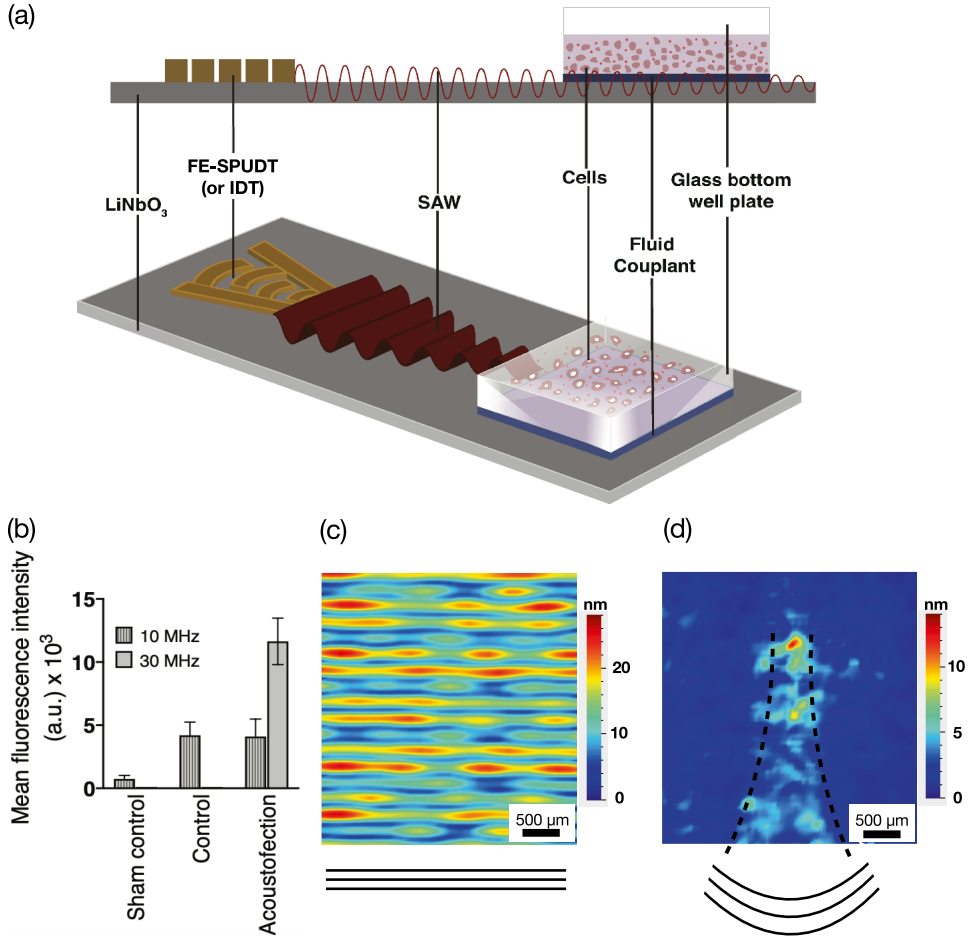

Figure 1. (a) Schematic illustrating the experimental setup in which a SAW, generated by applying an oscillating electric field to the FE-SPUDT (or IDT), which propagates along the $LiNbO_3$ substrate, is coupled through a fluid coupling layer into a glass-bottom well plate containing a suspension of cells and the transfection reagent. (b) Mean fluorescence intensity associated with emission from Cy3-labeled siRNA internalized in Jurkat cells with the 10 MHz IDT and 30 MHz FE-SPUDT devices. (c, d) Root-mean-square (RMS) surface displacement of the acoustic wave on the $LiNbO_3$ substrate patterned with the (c) 10 MHz IDT and (d) 30 MHz FE-SPUDT in the presence of the glass-bottom eight-well plate above, as obtained using the laser Doppler vibrometer (LDV).

nucleofection) and sonoporation, on the other hand, while effective, are known to inflict considerable irreversible damage to the cell membrane, leading to loss in homeostasis and, eventually, cell death. Cellular viabilities of around 70−80%, or even as low as 50−60%, are therefore not uncommon, for example, in electroporation due to the reliance of high electric potentials, or in sonoporation due to the large cavitational stresses required to trigger pore formation.[13−18]

Regardless of the technique employed, it is well known that suspension (nonadherent or trypsinized adherent) cells are notoriously hard to transfect.[19−22] In this study, we demonstrate the possibility of efficient transfection of siRNA in nonadherent Jurkat and HuT 78 cells—immortalized human peripheral blood T lymphoma cell lines commonly used to model patient-derived T cells. This is carried out by adapting a recently discovered acoustofection technique, in which high-frequency (10 MHz) surface acoustic waves (SAWs)[23−27] were shown to improve intracellular delivery of siRNA into adherent (human embryonic kidney (HEK293) and epithelial adenocarcinoma (HeLa)) cells.[28] More specifically, the acoustofection technique involved the irradiation of continuously distributed low amplitude (as opposed to short but very intense pulses[29]) MHz vibration associated with the SAW into cells. In particular, the SAW, while insufficient to either generate cavitation[30] and hence the formation of pores, was shown to drive transient structural reorganization of the lipids constituting the cell membrane that led to its permeabilization. This is unlike conventional as well as more recent nanoelectromechanical, microbubble, and microfluidic sonoporation techniques,[16,31−36] in which cavitational and other mechanical stresses are responsible for the formation of pores in the cell membrane to facilitate entry of therapeutic molecules. The absence of poration and the reversibility of the process (upon removal of the acoustic excitation, the cells were observed to rapidly—within minutes—relax back to their unexcited state) constitutes a significant advantage wherein considerably higher cell viabilities (>97%) were obtained. Moreover, unlike carrier-mediated methods that rely on endocytic uptake, the internalized therapeutic cargo was observed to be uniformly distributed throughout the cytoplasm instead of being localized in the endosomes and lysosomes. Consequently, the internalized molecules therefore have a higher probability of being trafficked to the nucleus.[28] A further advantage of the method is its speed, involving only 10 min of acoustic excitation, compared to the endocytosis process, which takes place over many hours. The acoustofection technique, however, has so far till now proven to be unsuccessful for suspension cells.

https://dx.doi.org/10.1021/acsabm.1c00003
ACS Appl. Bio Mater. 2021, 4, 2781−2789

Given the promise of RNA interference strategies in gene therapeutics (a number of which have advanced to phase III clinical trials[37−39]) together with long-standing challenges associated with its delivery—in particular, due to the cytotoxicity of a number of polymeric carriers, and their inability to overcome endosomal release,[40] we chose to deliver siRNA as a model therapeutic agent to be internalized into Jurkat and HuT 78 cells as proof-of-concept demonstration of this acoustofection technique. We benchmark the performance of our internalization method against nucleofection—the current commercial gold standard for intracellular delivery using a physical membrane disruption method,[41,42] and show comparable 2-fold enhancement in gene knockdown efficiency, but with considerably higher cell viability of around 91% (cf. approximately 76% with nucleofection). Moreover, the technique does not involve the extensive preparatory steps typically required for optimization of the nucleofection equipment, which is also comparatively more expensive in cost to the present acoustofection setup.

2. MATERIALS AND METHODS

2.1. Materials. A Nunc Lab-Tek CC2 chamber slide system, T25 cell culture flasks, standard glass-bottom 8-, 48-, and 96-well (square) plates, RNAse-free water, nuclease-free water, propidium iodide (PI), bovine serum albumin (BSA), fetal bovine serum (FBS), Dulbecco's phosphate-buffered saline (D-PBS), 4-(2-hydroxyethyl)-1-piperazineethanesulfonic acid (HEPES), glycerophosphate, Roswell Park Memorial Institute (RPMI-1640) medium, penicillin−streptomycin (Gibco), TrypLE reagent, Opti-MEM Reduced Serum medium, Silencer Cy3-labeled GAPDH siRNA, Silencer Negative Control siRNA, Human GAPDH TaqMan primer, human β-actin reverse transcription polymerase chain reaction (RT-PCR) primer, TRIzol reagent, Nonidet P-40, ethylenediaminetetraacetic acid (EDTA), Tris buffer Triton X-100, radioimmunoprecipitation (RIPA) assay buffer, Pierce ECL Western blotting detection reagent, Tris-buffered saline (TBST, 0.1% Tween 20), paraformaldehyde (PFA), nitrocellulose membrane (0.45 μm), protease inhibitor cocktail tablet, poly(acrylamide) gel, LIVE/DEAD Fixable Dead Cell stain, Hoechst 33342 nuclear stain, eBioscience Annexin V-FITC Apoptosis Detection Kit, Qiagen One-Step PCR Kit, RNase AWAY surface decontaminant, and Lipofectamine RNAiMAX reagent were acquired from Thermo Fischer Scientific Pty. Ltd. (Scoresby, VIC, Australia). Sodium chloride solution (NaCl), potassium chloride (KCl) solution, calcium chloride solution ($CaCl_2$), sodium fluoride (NaF) solution, sodium orthovanadate (Na_3VO_4), nonfat dry milk (NFDM), glycerin, glycerol, silicone oil, and dimethylsulfoxide (DMSO) were obtained from Sigma-Aldrich Pty. Ltd. (Castle Hill, NSW, Australia), whereas an SE Cell Line 4D-Nucleofector Kit was obtained from Lonza Pty. Ltd. (Mount Waverley, VIC, Australia). Primary (lysosome associated membrane glycoprotein 1 (LAMP1) rabbit monoclonal (9091S) and early endosome antigen 1 (EEA1) rabbit monoclonal (3288S)) and secondary (anti-rabbit Alexa fluor 488 (4412)) antibodies were purchased from Cell Signaling Technology (Danvers, MA). The following primers, procured from Integrated DNA Technologies, Inc. (Coralville, IA), were used for quantitative reverse transcription polymerase chain reaction (qRT-PCR):

- β-actin Forward: 5′-CACCATTGGCAATGAGCGGTTC-3′,
- β-actin Reverse: 5′-AGGTCTTTGCGGATGTCCACGT-3′
- GAPDH Forward: 5′- ACCACAGTCCATGCCATCAC-3′,
- GAPDH Reverse: 5′-TCCACCACCCTGTTGCTGTA-3′.

2.2. Cell Culture. Jurkat cells were cultured to 0.9−1 × 10^6/mL in RPMI-1640 medium supplemented with 20% heat-inactivated FBS, while HuT 78 cells were cultured in RPMI-1640 with 10% FBS; both cell lines were acquired from the American Type Culture Collection (ATCC, Rockville, MD). The cell media were supplemented with 1% penicillin−streptomycin (100 units/mL) and maintained at 37 °C and 5% CO_2. The cells (not used beyond passage 10), which were grown in a standard T25 flask that was kept upright throughout the study, were subsequently subcultured to a final density of 5 × 10^5 cells/mL by collecting them and spinning them down at 200g for 5 min. They were then seeded at a density of 1 × 10^5 cells/mL on 8-well chambered glass-bottom plates 48 h prior to the siRNA internalization experiments with either nucleofection or acoustofection for the stipulated duration prior to their removal for further analysis.

2.3. Acoustofection. Acoustofection was carried out by exposing the cells to the SAW using the setup shown in Figure 1a. The chipscale SAW device comprised a 127.86° Y−X rotated single-crystal piezoelectric lithium niobate ($LiNbO_3$) substrate on which either straight interdigitated transducer (IDT) or focusing-elliptical single-phase unidirectional transducer (FE-SPUDT) electrodes consisting of 60 alternating finger pairs of 10 nm chromium and 150 nm aluminum layers were patterned using standard UV photolithography and wet etching. We explored the use of two SAW frequencies f, i.e., 10 and 30 MHz, as specified by the SAW wavelength $\lambda_{SAW} = c/f$, which, in turn, is specified by the width and gap of the fingers d, wherein $d \approx \lambda_{SAW}/4$ for the straight IDT and $d \approx \lambda_{SAW}/8$, $3\lambda_{SAW}/8$, $\lambda_{SAW}/8$ for the SPUDT. For 10 and 30 MHz, $\lambda_{SAW} \approx 390$ and 133 μm, respectively.

To generate the propagating Rayleigh SAW on the $LiNbO_3$ substrate, we applied an alternating current with varying input voltages to the IDT or SPUDT using a signal generator (SML01, Rhode & Schwarz Pty. Ltd., North Ryde, NSW, Australia) and an amplifier (10W1000C, Amplifier Research, Souderton, PA). The vibrational energy was then coupled into each well in the chambered plate containing the cells (1 × 10^5 cells/mL, seeded 48 h prior) and reagents through a thin 10 μm layer of silicone oil (45−55 cP; 0.963 g/mL), as illustrated in Figure 1a, whose role was to minimize the acoustic impedance mismatch between the device and the well plate, so as to maximize energy transmission.[43] Spatiotemporal variations in the wave displacement amplitude along the substrate as well as the well floor were characterized using a laser Doppler vibrometer (LDV; UHF-120, Polytec GmBH, Waldbronn, Germany). Polystyrene particles (5 μm, Polysciences, Inc., Warrington, PA), on the other hand, were suspended in the media to visualize the effect of any flow or standing waves that arise within the well as a consequence of the acoustic wave transmission into it.

2.4. Nucleofection. For the benchmarking experiments using nucleofection, 1 × 10^5 cells/mL were seeded 48 h prior to transfection in a standard T25 flask. On the day of the transfection, the cell culture was prepared by filling in an appropriate number of wells with Opti-MEM Reduced Serum medium, preincubated in a humidified 37 °C/5% CO_2 incubator. The cells from the T25 flask were subsequently collected and centrifuged at 100g for 10 min to obtain a pellet with a density of 3 × 10^5 cells/mL. The master mix, to which the aforementioned cell pellet was added, comprised siRNA (20 nM) and the Nucleofector solution from the SE Cell Line 4D-Nucleofector Kit at room temperature. The master mix (20 μL) was then transferred to the Nucleocuvette strips supplied in the kit, and the appropriate manufacturer's preset program (i.e., Nucleofector conditions with varying pulse voltages and durations), optimized prior to the experiments according to the supplied protocol using plasmid DNA (positive pmaxGFP Vector supplied with the kit) to maximize both transfection efficiency and cell viability, was applied. A 4D-Nucleofector Core System (Lonza Pty. Ltd., Mount Waverley, VIC, Australia) consisting of X and Y units that accommodate both the cuvettes and strips was used for the nucleofection. Appropriate transfection controls involving negative (no siRNA) and untreated controls were also incorporated while optimizing the program conditions.

2.5. Viability and Cytotoxicity Assays. The LIVE/DEAD Fixable Aqua Dead Cell stain, which is based on the reaction of a fluorescent dye (with excitation and emission wavelengths of 367 and 526 nm, respectively) with amines that cannot penetrate live cell membranes but which readily penetrate damaged membranes in dead cells, was used to assess the viability of treated and untreated cell populations followed by fixation of the cells. The stain was prepared by mixing together one vial of the supplied fluorescent reactive dye

https://dx.doi.org/10.1021/acsabm.1c00003
ACS Appl. Bio Mater. 2021, 4, 2781−2789

and 50 μL of anhydrous DMSO well ahead of the experiments. Prior to the experiments, 1 μL of this stock solution was mixed with 125 μL of sterile PBS before adding them to the experimental samples. Nontransfected cells, heated to 55 °C for 60 min, served as the control containing a mixed population of live and dead cells. Single-stained (for siRNA alone) cells, LIVE/DEAD stained cells alone and both together were also included as part of the controls to establish the gating for flow cytometry. The cells were harvested from the well plates and spun down at 100*g* for 5 min, after which they were washed twice in fresh PBS. Unstained samples were resuspended in fresh sterile PBS, whereas the experimental samples were resuspended in 10 μL of the diluted dye and incubated for 20 min at room temperature. Sterile PBS (3 mL) was added to each tube, which was subsequently spun down for 5 min at 100*g*. The supernatant was then carefully removed, and the pellet was resuspended in 50 μL of FACS buffer (PBS, 1% FBS, and 1 mM EDTA at pH 8.0).

The degree of apoptosis in cells exposed to high powers and longer exposure times was evaluated using the eBioscience Annexin V-FITC Apoptosis Detection Kit. Cells were collected 48 h post treatment and washed twice in ice-cold PBS and centrifuged at 100*g* for 5 min. The spun-down cells were collected and resuspended in binding buffer (0.1 M HEPES/NaOH (pH 7.4), 1.4 M NaCl, 25 mM $CaCl_2$) at a concentration of 5×10^5 cells/mL with Annexin V-FITC (5 μL) to a final volume of 200 μL for 15 min in the dark. The cells were further washed in 500 μL binding buffer (1×) and resuspended in 190 μL containing 10 μL of PI (20 μg/mL), following which the cells were analyzed using flow cytometry (Accuri C6, BD BioSciences, San Jose, CA) without any further washing. The cells were kept on ice throughout up until the point of analysis.

2.6. Transfection Efficiency. *2.6.1. siRNA Uptake by Flow Cytometry.* Cell fluorescence due to the uptake of Cy3-labeled siRNA was analyzed using flow cytometry (Accuri C6, BD BioSciences, San Jose, CA). Briefly, 1×10^5 cells/mL were seeded 2 days prior to the transfection in eight-well chambered glass-bottom plates for the acoustofection experiments and in standard 48-well plates for the nucleofection experiments. On the day of transfection, the cells were collected and transfected according to the aforementioned acoustofection and nucleofection protocols. The cells were then left in the Opti-MEM Reduced Serum medium for 4 h, which was subsequently replaced with complete medium, after which they were collected for analysis at 24, 48, and 72 h. The collected samples were thrice washed in ice-cold PBS and spun down (5 min, 100*g*, 4 °C) into a pellet, which was then suspended in FACS buffer (PBS, 1% FBS, 1 mM EDTA pH 8.0). Cytometry was conducted at a wavelength of 488/532 nm.

2.6.2. Confocal Microscopy. For confocal laser scanning microscopy (N-STORM Super-Resolution Microscope, Nikon Corp., Tokyo, Japan), the cells were first washed twice in sterile PBS and fixed with 4% PFA for 10 min at room temperature, after which they were blocked using 10% goat serum for 1 h at room temperature. The cells were subsequently incubated with EEA1 and LAMP1 rabbit primary monoclonal antibodies, which are early endosome and lysosome markers, respectively, in 1% BSA (1:200 final concentration) overnight at 4 °C. The secondary antibody (anti-rabbit Alexa Fluor 488) was added to the washed cells (1:400 dilution) together with the nuclear stain (Hoechst 33342; 5 μM) in the last 5 min of the incubation period. The samples were finally washed thrice and loaded with fresh PBS prior to imaging. Control (unexposed) cells were maintained under the same conditions as that of the irradiated samples.

2.6.3. GAPDH Protein and Gene Profiling. Particular care was taken to clean the hoods and all consumables including pipettes and tip boxes with RNase AWAY surface decontaminant to avoid denaturation of the siRNA. The cells collected from the acoustofection experiments (same day) were twice washed in sterile PBS and the supernatant replaced with Opti-MEM Reduced Serum medium. A 1:5 molar ratio of siRNA to Lipofectamine RNAiMAX at a final concentration of 20 nM siRNA and 1 μL of Lipofectamine per 500 μL of Opti-MEM Reduced Serum medium was prepared prior to the experiments. The complex was incubated for 15 min at room temperature to form the siRNA−Lipofectamine complex, which was added to both untreated and treated samples simultaneously. The sham control consisted of cells in Opti-MEM Reduced Serum alone, whereas the scrambled siRNA control comprised cells transfected with siRNA containing random nucleotide sequences. Similar controls were employed for the nucleofection experiments, in which the cells were collected following treatment, washed twice in sterile PBS, and resuspended in complete medium on the day of the experiments. Both the acoustofection and nucleofection experiments were carried out at the same time.

For qRT-PCR (CFX96 Touch Real-Time PCR Detection System, Bio-Rad Laboratories, Inc., Hercules, CA), total RNA was extracted from the cells that were collected after 48 h using ethanol, isopropanol, and TRIzol; the RNA quantity was restricted to 250 ng per reaction while simultaneously maintaining the A_{260}/A_{280} ratio of the RNA between 1.9 and 2.2, as measured using a spectrophotometer (OPTIZEN Nano Q, Mecasys Co. Ltd., Daejeon, South Korea). This was then amplified with qRT-PCR using the Qiagen One-Step PCR Kit according to the manufacturer's instructions. Briefly, 250 ng of RNA was added to a mixture of 5× RT-PCR enzyme, 5× Q-solution, 10 nM dNTP mix, and the One-Step RT-PCR enzyme mix from the kit together with GAPDH primer and the experimental samples, including the controls and with β-actin primer as the housekeeping gene.

For the Western blot experiments, all of the experimental samples including the controls were harvested and spun down at 4000 rpm for 5 min. The supernatant was then discarded, and the cells were washed twice by spinning them down with fresh PBS at the same speed and duration. The cell pellet was resuspended with 500 μL of lysis buffer comprising 0.5% Nonidet P-40, 10 mM Tris (pH 7.5), 2.5 mM KCl, 0.5% Triton X-100, 150 mM NaCl, 30 mM glycerophosphate, 50 mM NaF, 1 mM Na_3VO_4, and 0.1% protease inhibitor mixture for every 1×10^6 cells/mL and incubated in a precooled rotor maintained at 4 °C for 2 h. The samples were further centrifuged for 30 min at 14 000 rpm, from which the protein concentration of the lysate was measured using the Bradford assay (Bio-Rad, Hercules, CA). Protein complex (2 μg) was then loaded onto a sodium dodecyl sulfate polyacrylamide gel (SDS-PAGE) and transferred to nitrocellulose membranes at 4 °C. The proteins were left on the membrane for 60 min and maintained at that temperature, following which they were incubated with the GAPDH primary and goat anti-rabbit GAPDH antibodies after blocking the membrane with BSA to reduce any nonspecific binding. The membranes were washed with TBST buffer for a minimum of three times and visualized using a gel imager (LI-COR Biotechnology, Lincoln, NE) following incubation in a Pierce ECL Western blotting detection reagent at room temperature for 2 min.

2.7. Statistical Analysis. Data presented in this study are expressed as mean ± standard deviation of replicate measurements, and one-way analysis of variance (ANOVA; Prism8, GraphPad software, San Diego, CA) was employed for comparisons where applicable.

3. RESULTS AND DISCUSSION

As the 10 MHz SAW device reported for intracellular siRNA delivery into adherent cells[28] failed to yield reasonable transfection efficiencies in nonadherent cells, we first explored the use of different SAW transducer configurations and frequencies to ascertain the SAW parameters that would provide a means for driving transmembrane molecular uptake of siRNA into the Jurkat and HuT 78 cells. In particular, we found the use of 30 MHz focused SAWs generated using the FE-SPUDT to facilitate superior siRNA internalization in these cells (Figure 1b). Given that suspension cells are likely to be dispersed throughout the well further from the acoustic source compared to adherent cells, which are attached to the base of the well, the use of focused excitation at higher frequencies is somewhat counterintuitive. This is because it would be reasonable to expect that the longer attenuation lengths

https://dx.doi.org/10.1021/acsabm.1c00003
ACS Appl. Bio Mater. 2021, 4, 2781−2789

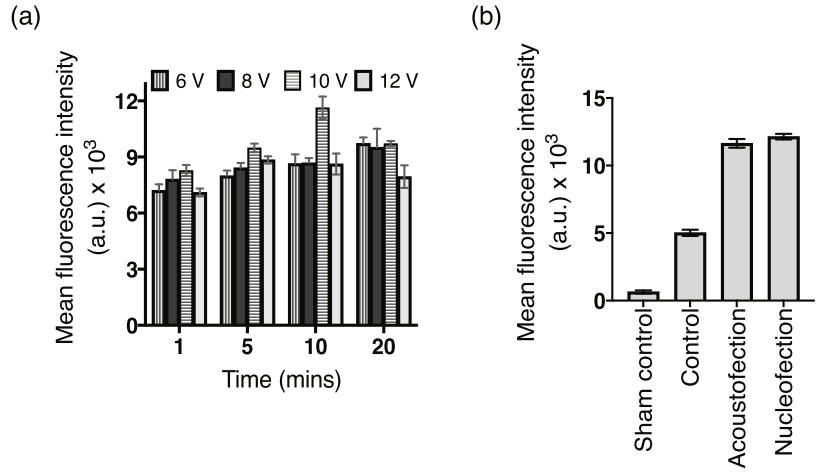

Figure 2. (a) Mean fluorescence intensity associated with emission from Cy3-labeled siRNA internalized in Jurkat cells with the acoustofection technique under different exposure times and input voltages, as measured through flow cytometry. (b) Comparison of the uptake efficiency of Cy3-labeled siRNA in Jurkat cells, as measured by the mean fluorescence intensity from the flow cytometry analysis, between the acoustofection (10 V, 10 min) and nucleofection (CM-137) techniques. The sham control is devoid of siRNA and the acoustofection or nucleofection treatments, while the control comprises Lipofectamine RNAiMAX that aids internalization of the siRNA via endocytosis.

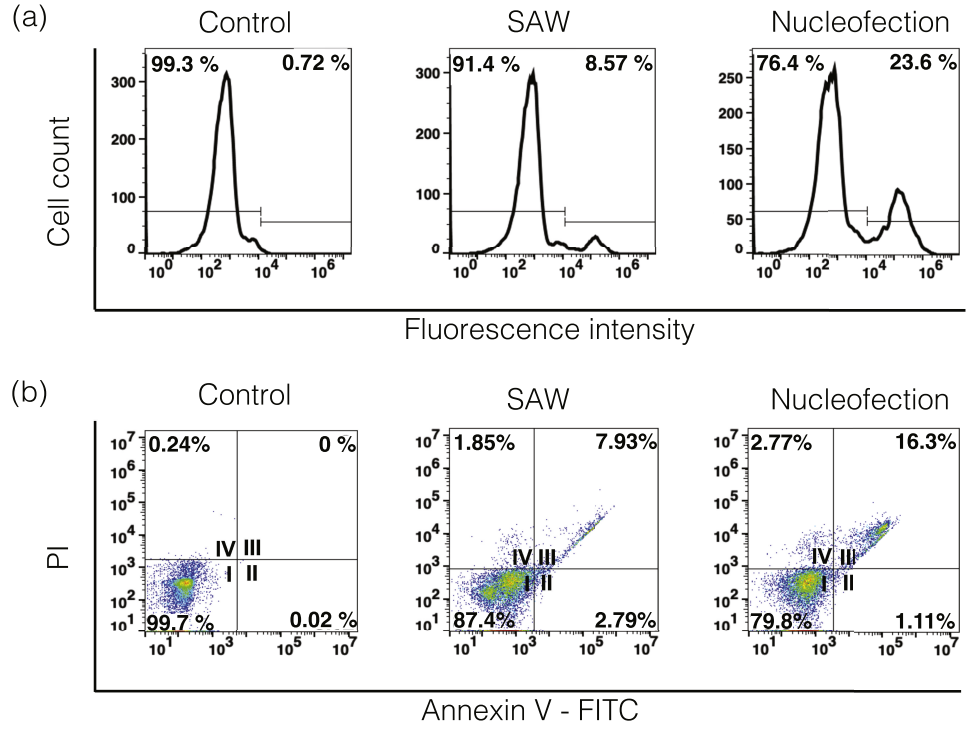

Figure 3. (a) Viability of LIVE/DEAD stained Jurkat cells associated with the unexposed control, and following acoustofection (10 V, 10 min) and nucleofection (CM-137), as measured through flow cytometry. (b) Representative dot plots following Annexin V/PI dual staining of unexposed (control), acoustofected (10 V, 10 min), and nucleofected (CM-137) Jurkat cells, as obtained via flow cytometry, identifying populations of live cells (quadrant 1: Annexin V−/PI−), early apoptotic cells (quadrant 2: Annexin V+/PI−), late apoptotic/necrotic cells (quadrant 3: Annexin V +/PI+), and dead cells (quadrant 4; Annexin V−/PI+).

associated with the lower 10 MHz excitation frequency, and a more broadly distributed acoustic transmission path produced by the straight IDT (Figure 1c) compared to that associated with the narrowly focused beam produced by the FE-SPUDT (Figure 1d), would be more efficient for coupling the vibrational energy to suspension cells dispersed throughout the well. Nevertheless, this premise is predicated on the (mis)assumption that it is the acoustic radiation pressure that is the predominant mechanism by which the vibrational energy is transmitted to the cells to effect the intracellular transport.

Inspection of the respective flow patterns produced by the respective 10 MHz IDT and 30 MHz FE-SPUDT configurations (Supporting Information Figure S1), however, reveals that the 10 MHz IDT acoustic irradiation, due to its longer attenuation path length (≈4.7 mm) and distributed transmission path spanning the entire lateral dimension of the well, produces strong reflections across the well, whose superimposition sets up a dominant standing wave within the well (Figure 1c) that suppresses the flow (acoustic streaming). This can be visualized by the particle aggregates that form along the

https://dx.doi.org/10.1021/acsabm.1c00003
ACS Appl. Bio Mater. 2021, 4, 2781−2789

nodal lines of the standing wave in Supporting Information Figure S1a. In contrast, these linear particle aggregates appear to be absent for the case of the 30 MHz FE-SPUDT (Supporting Information Figure S1b). This is because the shorter attenuation path length (≈1.6 mm) and narrow-focused acoustic transmission path associated with this electrode configuration (Figure 1d) give rise to stronger acoustic streaming that dominates over any weak standing-wave effects to erase any particle patterns that may arise. As such, we postulate that the dominant mechanism by which the vibrational energy is coupled from the piezoelectric substrate through the well and the media to the suspended cells is via second-order flow (acoustic streaming) effects as opposed to direct first-order (acoustic radiation pressure) transmission. This is likely because suspension cells, just like the synthetic particles used for the visualization, are likely to be trapped as linear aggregates at the nodal positions of any standing waves that form within the well, where, given the nature of an acoustic wave node, they do not feel the effect of any vibration (we note that although the linear aggregates were observed for a system with synthetic particles, it is well known that cells behave in a similar manner[24,26]).

The siRNA transfection results in Jurkat and HuT 78 cells that we report henceforth were therefore obtained using the 30 MHz FE-SPUDT device. To benchmark the performance of this acoustofection technique, we compare our results with that obtained using nucleofection—long considered the commercial gold standard for transfection via physical membrane disruption.[41,42] In nucleofection, transport across the cell membrane is enabled through the formation of pores in the membrane by the application of an intense electric field (typically 10^{-1}–10^{2} kV/cm) over a short pulse duration (between 1 ns and 1 s).[44] To determine the best operating conditions for the nucleofection experiments, we first carried out preliminary experiments with the different manufacturer's preset programs (i.e., Nucleofector conditions with varying pulse voltages and durations) according to the supplied optimization protocol to maximize both cell viability and transfection efficiency for uptake of the green fluorescent protein (GFP) plasmid supplied with the Nucleofector kit. As can be seen from the results in Supporting Information Figure S2b, the CM-137 program provided the best transfection and cell viability, and thus was used in all of the siRNA transfection experiments that we report henceforth.

Figure 2a and Supporting Information Figure S3 show the uptake of Cy3-conjugated siRNA in Jurkat and HuT 78 cells, respectively, as a function of both the SAW input voltage and exposure duration, as confirmed through flow cytometry. Both show an increase in internalization of the siRNA, not only with respect to the unexposed control but also with increasing input voltage and exposure duration, although we note that an optimum exists at approximately 10 V and 10 min due to a decrease in cell viability as a consequence of excessive irradiation over prolonged exposure times. As such, we conducted all subsequent acoustofection experiments at this optimum input voltage and exposure duration, for which we obtained cell viabilities of approximately 91% (Figure 3a). This is considerably higher than that obtained with nucleofection under optimized conditions (around 76%; Figure 3a) with which we obtained comparable uptake efficiencies, wherein both acoustofection and nucleofection were observed to lead to greater than 2-fold increases in siRNA uptake compared to the unexposed control (Figure 2b).

The Annexin V/PI double-staining assay, which allows us to determine if the approximately 8% decrease in viability to that of the control (approximately 99%; Figure 3a) was due to cell apoptosis, nevertheless showed no significant difference (≈1.5%) for both acoustofection and nucleofection in early apoptotic (quadrant 2 in Figure 3b) and necrotic (quadrant 4 in Figure 3b) cells compared to that for the control, although the nucleofected samples (16.3%) appeared to be around two times higher than that of the acoustofected cells (7.93%) for late apoptotic cells (quadrant 3 in Figure 3b). The emergence of high apoptosis levels in the later stages of transfection can be attributed to the loss of cell membrane and mitochondrial integrity due to DNA fragmentation, which eventually leads to cell death.[45] Overall, we note that the cumulative increase in the apoptotic cells in the nucleofected samples was approximately twice (20.18%) that of the acoustofected cells (12%) for comparable uptake efficiencies; the degree of apoptosis in the acoustofected cells being comparable to that for the nucleofected cells even at the highest acoustofection input power and exposure duration (Supporting Information Figure S4). These results therefore allude to the superiority of the acoustofection technique, at least in terms of preserving cell viability, which can be attributed to the absence of pore formation in the cells and since the reorganization of the lipid structure that leads to permeabilization of the cell membrane to allow through passage and hence uptake of the siRNA is temporal and reversible (i.e., the cell membrane reverts to its original state upon relaxation of the acoustic excitation),[28] consistent with prior findings of the reversibility in early apoptosis in terms of the ability of the cells to recover.[46]

The confocal microscopy images in Figure 4 show that the siRNA that was internalized in cells stained for both early endosomes (EEA1) and lysosomes (LAMP1) under both acoustofection and nucleofection appear to be distributed throughout the cytoplasm, as observed from the punctate appearance of the overlapping signals (yellow) between the siRNA fluorescence (red) and the early endosome and lysosome stains (green). This is in distinct contrast to the unexposed control, in which the overlap was considerably more pronounced, indicating significant co-localization of the siRNA within the endosomes and lysosomes due to endocytic uptake. Quantification of the extent of co-localization of the internalized siRNA with both the early endosomal and lysosomal regions using image analysis (Supporting Information Figure S5) confirms considerably lower endosomal/lysosomal trapping with the acoustofection (60.6 ± 3.8%) and nucleofection (71.4 ± 2.0%) techniques normalized against that of the control (100%). These observations are consistent with our current understanding of the internalization mechanism associated with the acoustofection technique.[28] Similar to the poration mechanisms responsible for internalization in nucleofection, albeit without the formation of physical pores, the transient membrane permeabilization arising from the acoustic irradiation of the cell facilitates direct entry of the siRNA into the cytoplasm, thus avoiding trapping of the cargo within the endosomal and lysosomal compartments and hence circumventing the need for endosomal escape strategies. The fact that endocytosis is not the dominant uptake mechanism in the acoustofected cells is also confirmed by the insensitivity of the results to various endocytosis inhibitors[28] and the much faster internalization times (10 min), especially since the endocytosis process typically requires significantly longer durations (many hours). In any case, the

https://dx.doi.org/10.1021/acsabm.1c00003
ACS Appl. Bio Mater. 2021, 4, 2781−2789

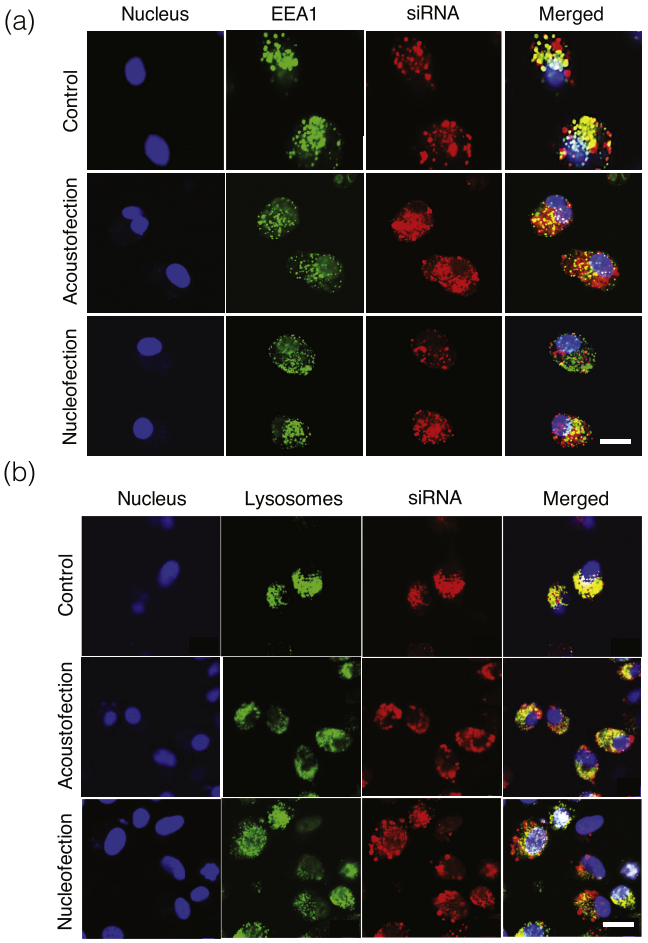

Figure 4. Confocal microscopy images of Jurkat cells 4 h after transfection with Cy3-labeled GAPDH siRNA (red) after acoustofection (10 V, 10 min) and nucleofection (CM-137) compared to the unexposed control, following staining with (a) an early endosomal marker EEA1 and (b) the lysosomal-associated membrane protein LAMP1, both of which are displayed by the green channels. Cell nuclei were stained by Hoechst 3342 (blue), and the overlay in the last column comprised a merger of the individual channels showing the localization (or lack thereof, for the acoustofected cells) of the internalized siRNA in the endosomal and lysosomal compartments; the extent of such co-localization, quantified using image analysis, is reported in Supporting Information Figure S5. The scale bars represent 20 μm lengths.

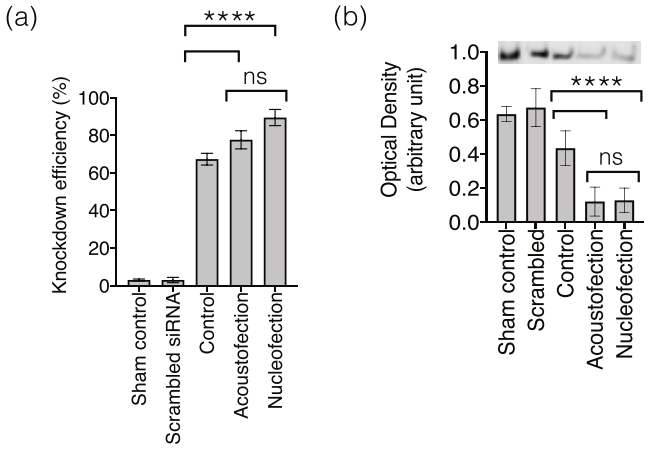

Figure 5. (a) GAPDH knockdown efficiency, as measured through GAPDH mRNA expression with qRT-PCR, following acoustofection (10 V, 10 min) and nucleofection (CM-137) of GAPDH siRNA in Jurkat cells. (b) Densitometry plots showing the GAPDH protein levels following acoustofection (10 V, 10 min) and nucleofection (CM-137) treatment of the Jurkat cells, obtained from the Western blot data (inset: lanes correspond to the cases denoted by the *x*-axis labels in the plot below). The data are represented in terms of the mean (n = 3) ± the standard deviation. The asterisks **** indicate statistically significant differences with $p < 0.0001$. In both (a) and (b), the controls comprise cells unexposed to either acoustofection or nucleofection; the sham control is devoid of siRNA, whereas the scrambled control consisted of cells transfected with siRNA containing random nucleotide sequences.

cytosolic delivery afforded by the acoustofection technique is a significant advantage in terms of enhancing transfection efficiency given that the cytosol constitutes the target destination for the RNA silencing pathway[47,48] and since there are intracellular pathways to traffic the internalized molecules directly to the nucleus (such as in epigenetic silencing).[10,49,50]

Quantitative analysis of mRNA cleavage through the total extracted RNA from siRNA-transfected Jurkat cells showed 77 and 89% reductions in the expression of GAPDH mRNA for the acoustofected and nucleofected cells, respectively, compared to the unexposed sham control (Figure 5a). For HuT 78 cells, the knockdown efficiencies were 86 and 91%, respectively (Supporting Information Figure S6). No silencing was observed in samples treated with the scrambled control; we note some silencing occurs in the control given that they contain the same nucleotide composition together with a chemical transfection agent Lipofectamine RNAiMAX that aids internalization of the siRNA via endocytosis for comparison. These results are consistent with the approximate 2-fold reduction in the GAPDH protein expression for the acoustofected and nucleofected cells in both Jurkat and HuT 78 cells, as seen from the Western blot results (Figure 5b and Supporting Information Figure S6b, respectively), indicating successful mRNA knockdown by the RNA-induced silencing complex (RISC).

4. CONCLUSIONS

We have demonstrated the possibility of enhancing intracellular delivery and hence transfection in difficult-to-transfect nonadherent cell lines such as suspension T cells with a recently developed acoustofection technique involving low-power, high-frequency (30 MHz) vibration of the cells. The technique is rapid, requiring just 10 min of exposure, and does not involve the generation of pores in the cell membrane given the absence of cavitation at high frequencies and low excitation powers.[30] Rather, the gentle vibration of the cells drives a temporal reorganization of the cell membrane's lipid structure that increases its permeability, thereby facilitating ease of molecular transport across the membrane; this process is reversible and the lipid structure immediately relaxes to its original state upon removal of the excitation. Consequently, we observe markedly higher cell viabilities (>91%) compared to poration-based techniques (e.g., electroporation, sonoporation, and optoporation). Moreover, unlike endocytic-driven uptake, which is the primary internalization mechanism associated with biochemical carrier-mediated transport, the internalized therapeutic cargo is observed to be distributed throughout the cell instead of being localized within the endosomes and lysosomes, therefore permitting easier and more efficient

https://dx.doi.org/10.1021/acsabm.1c00003
ACS Appl. Bio Mater. 2021, 4, 2781−2789

trafficking to the nucleus for transfection without being degraded. This is reflected by the approximate 2-fold increase in transfection efficiency that we observe in siRNA uptake experiments, which is comparable to that observed with nucleofection (electroporation) but with considerably higher (around 15%) cell viabilities. As such, the acoustofection technique therefore constitutes a simple, rapid, and scalable (see, for example, ref 51, where the technology is parallelized to address each of the chambers in a 96-well microarray plate) means for effective nonviral intracellular delivery and hence transfection of adherent as well as nonadherent cells while maintaining the high cell viabilities critical for ex vivo autologous therapeutics.

■ ASSOCIATED CONTENT

Supporting Information

The Supporting Information is available free of charge at https://pubs.acs.org/doi/10.1021/acsabm.1c00003.

Visualization experiments showing the effect of standing waves (if any) produced by the IDT configuration on particle trapping (Figure S1); optimization of acoustofection and nucleofection parameters (Figure S2); siRNA internalization in HuT 78 cells (Figure S3); flow cytometry analysis (Figure S4); extent of colocalization of internalized siRNA with the early endosomal and lysosomal regions (Figure S5); and siRNA knockdown in HuT 78 cells (Figure S6) (PDF)

■ AUTHOR INFORMATION

Corresponding Author

Leslie Y. Yeo − *Micro/Nanophysics Research Laboratory, School of Engineering, RMIT University, Melbourne, VIC 3000, Australia;* orcid.org/0000-0002-5949-9729; Email: leslie.yeo@rmit.edu.au

Authors

Shwathy Ramesan − *Micro/Nanophysics Research Laboratory, School of Engineering, RMIT University, Melbourne, VIC 3000, Australia*

Amgad R. Rezk − *Micro/Nanophysics Research Laboratory, School of Engineering, RMIT University, Melbourne, VIC 3000, Australia;* orcid.org/0000-0002-3556-5621

Paula M. Cevaal − *The Peter Doherty Institute for Infection and Immunity, University of Melbourne and Royal Melbourne Hospital, Melbourne, VIC 3000, Australia;* orcid.org/0000-0003-4473-7904

Christina Cortez-Jugo − *Department of Chemical Engineering, University of Melbourne, Parkville, VIC 3010, Australia*

Jori Symons − *The Peter Doherty Institute for Infection and Immunity, University of Melbourne and Royal Melbourne Hospital, Melbourne, VIC 3000, Australia;* orcid.org/0000-0001-6560-1577

Complete contact information is available at: https://pubs.acs.org/10.1021/acsabm.1c00003

Notes

The authors declare no competing financial interest.

■ ACKNOWLEDGMENTS

L.Y.Y. acknowledges funding from the Australian Research Council (ARC) through Discovery Project grant DP170101061. The authors thank Dr. Zeyad Nasa for technical assistance with the use of the facilities at the RMIT MicroNano Research Facility.

■ REFERENCES

(1) Stewart, M. P.; Sharei, A.; Ding, X.; Sahay, G.; Langer, R.; Jensen, K. F. In vitro and ex vivo strategies for intracellular delivery. *Nature* **2016**, *538*, 183−192.

(2) Barua, S.; Mitragotri, S. Challenges associated with penetration of nanoparticles across cell and tissue barriers: a review of current status and future prospects. *Nano Today* **2014**, *9*, 223−243.

(3) Li, H.; Yang, Y.; Hong, W.; Huang, M.; Wu, M.; Zhao, X. Applications of genome editing technology in the targeted therapy of human diseases: mechanisms, advances and prospects. *Signal Transduction Targeted Ther.* **2020**, *5*, No. 1.

(4) Tay, A.; Melosh, N. Nanostructured materials for intracellular cargo delivery. *Acc. Chem. Res.* **2019**, *52*, 2462−2471.

(5) O'Brien, K.; Breyne, K.; Ughetto, S.; Laurent, L. C.; Breakefield, X. O. RNA delivery by extracellular vesicles in mammalian cells and its applications. *Nat. Rev. Mol. Cell Biol.* **2020**, *21*, 585−606.

(6) Pack, D. W.; Hoffman, A. S.; Pun, S.; Stayton, P. S. Design and development of polymers for gene delivery. *Nat. Rev. Drug Discovery* **2005**, *4*, 581−593.

(7) Kanasty, R.; Dorkin, J. R.; Vegas, A.; Anderson, D. Delivery materials for siRNA therapeutics. *Nat. Mater.* **2013**, *12*, 967−977.

(8) Mitragotri, S.; Burke, P. A.; Langer, R. Overcoming the challenges in administering biopharmaceuticals: formulation and delivery strategies. *Nat. Rev. Drug Discovery* **2014**, *13*, 655−672.

(9) Torchilin, V. P. Recent approaches to intracellular delivery of drugs and DNA and organelle targeting. *Annu. Rev. Biomed. Eng.* **2006**, *8*, 343−375.

(10) Sahay, G.; Alakhova, D. Y.; Kabanov, A. V. Endocytosis of nanomedicines. *J. Controlled Release* **2010**, *145*, 182−195.

(11) Shirley, J. L.; de Jong, Y. P.; Terhorst, C.; Herzog, R. W. Immune responses to viral gene therapy vectors. *Mol. Ther.* **2020**, *28*, 709−722.

(12) Zakeri, A.; Kouhbanani, M. A. J.; Beheshtkhoo, N.; Beigi, V.; Mousavi, S. M.; Hashemi, S. A. R.; Zade, A. K.; Amani, A. M.; Savardashtaki, A.; Mirzaei, E.; Jahandideh, S.; Movahedpour, A. Polyethylenimine-based nanocarriers in co-delivery of drug and gene: a developing horizon. *Nano Rev. Exp.* **2018**, *9*, No. 1488497.

(13) Feril, L. B.; Kondo, T.; Zhao, Q.-L.; Ogawa, R.; Tachibana, K.; Kudo, N.; Fujimoto, S.; Nakamura, S. Enhancement of ultrasound-induced apoptosis and cell lysis by echo-contrast agents. *Ultrasound Med. Biol.* **2003**, *29*, 331−337.

(14) Li, S. Electroporation gene therapy: new developments in vivo and in vitro. *Curr. Gene Ther.* **2004**, *4*, 309−316.

(15) Fox, M.; Esveld, D.; Valero, A.; Luttge, R.; Mastwijk, H.; Bartels, P.; van den Berg, A.; Boom, R. Electroporation of cells in microfluidic devices: a review. *Anal. Bioanal. Chem.* **2006**, *385*, No. 474.

(16) Qiu, Y.; Zhang, C.; Tu, J.; Zhang, D. Microbubble-induced sonoporation involved in ultrasound-mediated DNA transfection in vitro at low acoustic pressures. *J. Biomech.* **2012**, *45*, 1339−1345.

(17) Zhang, Z.; Qiu, S.; Zhang, X.; Chen, W. Optimized DNA electroporation for primary human T cell engineering. *BMC Biotechnol.* **2018**, *18*, No. 4.

(18) Yun, H.; Hur, S. C. Sequential multi-molecule delivery using vortex-assisted electroporation. *Lab Chip* **2013**, *13*, 2764−2772.

(19) Phillips, A. J. The challenge of gene therapy and DNA delivery. *J. Pharm. Pharmacol.* **2001**, *53*, 1169−1174.

(20) Praveen, B. B.; Stevenson, D. J.; Antkowiak, M.; Dholakia, K.; Gunn-Moore, F. J. Enhancement and optimization of plasmid expression in femtosecond optical transfection. *J. Biophotonics* **2011**, *4*, 229−235.

(21) Basiouni, S.; Fuhrmann, H.; Schumann, J. High-efficiency transfection of suspension cell lines. *BioTechniques* **2012**, *53*, 1−4.

(22) Cao, Y.; Ma, E.; Cestellos-Blanco, S.; Zhang, B.; Qiu, R.; Su, Y.; Doudna, J. A.; Yang, P. Nontoxic nanopore electroporation for effective intracellular delivery of biological macromolecules. *Proc. Natl. Acad. Sci. U.S.A.* **2019**, *116*, 7899−7904.
(23) Friend, J.; Yeo, L. Y. Microscale acoustofluidics: microfluidics driven via acoustics and ultrasonics. *Rev. Mod. Phys.* **2011**, *83*, 647−704.
(24) Ding, X.; Li, P.; Lin, S.-C. S.; Stratton, Z. S.; Nama, N.; Guo, F.; Slotcavage, D.; Mao, X.; Shi, J.; Costanzo, F.; Huang, T. J. Surface acoustic wave microfluidics. *Lab Chip* **2013**, *13*, 3626−3649.
(25) Yeo, L. Y.; Friend, J. F. Surface acoustic wave microfluidics. *Annu. Rev. Fluid Mech.* **2014**, *46*, 379−406.
(26) Destgeer, G.; Sung, H. J. Recent advances in microfluidic actuation and micro-object manipulation via surface acoustic waves. *Lab Chip* **2015**, *15*, 2722−2738.
(27) Go, D. B.; Atashbar, M. Z.; Ramshani, Z.; Chang, H.-C. Surface acoustic wave devices for chemical sensing and microfluidics: a review and perspective. *Anal. Methods* **2017**, *9*, 4112−4134.
(28) Ramesan, S.; Rezk, A. R.; Dekiwadia, C.; Cortez-Jugo, C.; Yeo, L. Y. Acoustically-mediated intracellular delivery. *Nanoscale* **2018**, *10*, 13165−13178.
(29) Yoon, S.; Kim, M. G.; Chiu, C. T.; Hwang, J. Y.; Kim, H. H.; Wang, Y.; Shung, K. K. Direct and sustained intracellular delivery of exogenous molecules using acoustic-transfection with high frequency ultrasound. *Sci. Rep.* **2016**, *6*, No. 20477.
(30) Rezk, A. R.; Ahmed, H.; Brain, T. L.; Castro, J. O.; Tan, M. K.; Langley, J.; Cox, N.; Mondal, J.; Li, W.; Ashokkumar, M.; Yeo, L. Y. Free radical generation from high-frequency electromechanical dissociation of pure water. *J. Phys. Chem. Lett.* **2020**, *11*, 4655−4661.
(31) Mehier-Humbert, S.; Bettinger, T.; Yan, F.; Guy, R. H. Plasma membrane poration induced by ultrasound exposure: implication for drug delivery. *J. Controlled Release* **2005**, *104*, 213−222.
(32) Prentice, P.; Cuschieri, A.; Dholakia, K.; Prausnitz, M.; Campbell, P. Membrane disruption by optically controlled microbubble cavitation. *Nat. Phys.* **2005**, *1*, 107−110.
(33) Zhang, Z.; Wang, Y.; Zhang, H.; Tang, Z.; Liu, W.; Lu, Y.; Wang, Z.; Yang, H.; Pang, W.; Zhang, H.; Zhang, D.; Duan, X. Hypersonic poration: a new versatile cell poration method to enhance cellular uptake using a piezoelectric nano-electromechanical device. *Small* **2017**, *13*, No. 1602962.
(34) Meng, L.; Liu, X.; Wang, Y.; Zhang, W.; Zhou, W.; Cai, F.; Li, F.; Wu, J.; Xu, L.; Niu, L.; Zheng, H. Sonoporation of cells by a parallel stable cavitation microbubble array. *Adv. Sci.* **2019**, *6*, No. 1900557.
(35) Belling, J. N.; Heidenreich, L. K.; Tian, Z.; Mendoza, A. M.; Chiou, T.-T.; Gong, Y.; Chen, N. Y.; Young, T. D.; Wattanatorn, N.; Park, J. H.; Scarabelli, L.; Chiang, N.; Takahashi, J.; Young, S. G.; Stieg, A. Z.; De Oliveira, S.; Huang, T. J.; Weiss, P. S.; Jonas, S. J. Acoustofluidic sonoporation for gene delivery to human hematopoietic stem and progenitor cells. *Proc. Natl. Acad. Sci. U.S.A.* **2020**, *117*, 10976−10982.
(36) Stride, E.; Coussios, C. Nucleation, mapping and control of cavitation for drug delivery. *Nat. Rev. Phys.* **2019**, *1*, 495−509.
(37) Nikam, R. R.; Gore, K. R. Journey of siRNA: clinical developments and targeted delivery. *Nucleic Acid Ther.* **2018**, *28*, 209−224.
(38) Morrison, C. Alnylam prepares to land first RNAi drug approval. *Nat. Rev. Drug Discovery* **2018**, *17*, 156−157.
(39) Garber, K. Alnylam launches era of RNAi drugs. *Nat. Biotechnol.* **2018**, *36*, 777−778.
(40) Whitehead, K. A.; Langer, R.; Anderson, D. G. Knocking down barriers: advances in siRNA delivery. *Nat. Rev. Drug Discovery* **2009**, *8*, 129−138.
(41) Wayteck, L.; Xiong, R.; Braeckmans, K.; De Smedt, S. C.; Raemdonck, K. Comparing photoporation and nucleofection for delivery of small interfering RNA to cytotoxic T cells. *J. Controlled Release* **2017**, *267*, 154−162.
(42) Ramishetti, S.; Peer, D. Engineering lymphocytes with RNAi. *Adv. Drug Delivery Rev.* **2019**, *141*, 55−66.
(43) Hodgson, R. P.; Tan, M.; Yeo, L.; Friend, J. Transmitting high power rf acoustic radiation via fluid couplants into superstrates for microfluidics. *Appl. Phys. Lett.* **2009**, *94*, No. 024102.
(44) Weaver, J. C.; Smith, K. C.; Esser, A. T.; Son, R. S.; Gowrishankar, T. A brief overview of electroporation pulse strength-duration space: a region where additional intracellular effects are expected. *Bioelectrochemistry* **2012**, *87*, 236−243.
(45) Elmore, S. Apoptosis: a review of programmed cell death. *Toxicol. Pathol.* **2007**, *35*, 495−516.
(46) Geske, F.; Lieberman, R.; Strange, R.; Gerschenson, L. Early stages of p53-induced apoptosis are reversible. *Cell Death Differ.* **2001**, *8*, 182−191.
(47) Shim, M. S.; Kwon, Y. J. Controlled cytoplasmic and nuclear localization of plasmid DNA and siRNA by differentially tailored polyethylenimine. *J. Controlled Release* **2009**, *133*, 206−213.
(48) Whitehead, K. A.; Dahlman, J. E.; Langer, R. S.; Anderson, D. G. Silencing or stimulation? siRNA delivery and the immune system. *Annu. Rev. Chem. Biomol. Eng.* **2011**, *2*, 77−96.
(49) Sahay, G.; Querbes, W.; Alabi, C.; Eltoukhy, A.; Sarkar, S.; Zurenko, C.; Karagiannis, E.; Love, K.; Chen, D.; Zoncu, R.; Buganim, Y.; Schroeder, A.; Langer, R.; Anderson, D. G. Efficiency of siRNA delivery by lipid nanoparticles is limited by endocytic recycling. *Nat. Biotechnol.* **2013**, *31*, 653−658.
(50) Gilleron, J.; Querbes, W.; Zeigerer, A.; Borodovsky, A.; Marsico, G.; Schubert, U.; Manygoats, K.; Seifert, S.; Stöter, C.; Epstein-Barash, H.; Zhang, L.; Koteliansky, V.; Fitzgerald, K.; Fava, E.; Bickle, M.; Kalaidzidis, Y.; Akinc, A.; Maier, M.; Zerial, M.; et al. Image-based analysis of lipid nanoparticle-mediated siRNA delivery, intracellular trafficking and endosomal escape. *Nat. Biotechnol.* **2013**, *31*, 638−646.
(51) Rezk, A. R.; Ramesan, S.; Yeo, L. Y. Plug-and-actuate on demand: multimodal individual addressability of microarray plates using modular hybrid acoustic wave technology. *Lab Chip* **2018**, *18*, 406−411.

https://dx.doi.org/10.1021/acsabm.1c00003
ACS Appl. Bio Mater. 2021, 4, 2781−2789